ACS APPLIED MATERIALS & INTERFACES

RESEARCH ARTICLE

www.acsami.org

Solvothermal Preparation of Pd Nanostructures under Nitrogen and Air Atmospheres and Electrocatalytic Activities for the Oxidation of Methanol

Haiyan Sun, Xiuling Jiao,* Hanyu Wang, Zhen Jiang, and Dairong Chen*

Key Laboratory for Special Functional Aggregate Materials of Education Ministry, School of Chemistry & Chemical Engineering, Shandong University, Jinan 250100 P. R. China

Supporting Information

ABSTRACT: Monodispersed Pd nanoparticles and their porous sphere-like aggregates with different lattice parameters were solvothermally prepared under nitrogen and air atmospheres. Here $PdCl_2$ acted as Pd precursor and hexadecylamine played the roles of solvent, reductant, and surface capping agent. Oxygen existing in air resulted in the change of surface capping agent, which then induced the aggregation of Pd nanoparticles, and the incorporation of oxygen led to the expansion of its lattice parameter to 0.398 nm, whereas the standard lattice parameter in metallic Pd is 0.389 nm. The monodispersed nanoparticles presented better catalytic activity and stability for the oxidation of methanol than the sphere-like Pd aggregates.

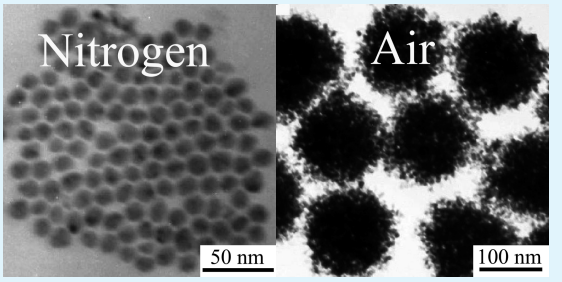

KEYWORDS: palladium, monodispersed nanoparticle, porous sphere-like aggregates, reaction atmosphere, electrocatalyst, methanol oxidation

INTRODUCTION

The syntheses of Pd nanostructures with controlled shapes have been extensively studied in the past decades owing to their unique properties and remarkable performance in many applications, such as catalysis,[1,2] hydrogen storage,[3,4] and hydrogen sensors.[5−8] Controlling the shape or morphology of metal nanostructures provides effective means of tuning their optical, electronic, magnetic, and catalytic properties.[9−14] The catalytic activity strongly depends on the size and shape of the metal nanoparticles, so the nature of the active sites becomes crucial in understanding the reactivity. For example, compared to larger Pd particles, smaller ones present better catalytic activity toward the coupling of 1-chloro-4-nitrobenzene with phenylboronic acid due to larger surface area.[15] And the catalytic activity increases with the fraction of surface atoms at the corners and edges, implying the morphology of the nanoparticles could influence its catalysis.[16] In addition, the stabilizer such as polymer and surfactant can also affect the catalytic activity of Pd nanoparticles. It diminishes the Ostwald ripening process by capping many of the free metallic surface sites.[17] It is observed that the catalytic activity decreased for the diminished accessibility of the metallic atoms at the surface.[18] Therefore, controlled synthesis of Pd nanostructure has not only the fundamental importance but also the practical application.

Much effort has been devoted to the fabrication of Pd nanostructures with different morphologies and sizes, such as nanoparticle,[19−21] nanorod,[22−24] nanobar,[23] nanowire,[22,25] nanoplates,[26] and also three-dimensional nanostructures.[27,28] In solution reactions, surfactants,[25,29] polymer molecules[30] or RNAs usually mediate the reaction.[31,32] The surfactants or polymers could stabilize the nanoparticles and direct their growth and a coordinating ligand or capping agent may selectively interact with the special facets of palladium, which may have synergistic effects on the order of free energy of different facets, changing their relative growth rates and resulting in the different final shapes.[33,34] And the parameters to control the shape or size of palladium nanostructures generally include the concentration of Pd precursor,[15,35] the reaction temperature,[35] the reaction time,[20,33] the pH value of initial mixtures,[15] the kind of solvents,[25] the structure of the surfactant or polymer or adding foreign ions.[15,22,29,36] Generally, in these syntheses, controlling the kinetic process is the preferable approach to tune their shape or morphology. Reaction atmosphere may play a significant role in chemical synthesis. For example, Li et al prepared Pt/C and PtRu/C nanoparticles in a polyol process, finding that the reaction atmosphere could affect the oxidation-state species in the active components of the catalysts and their electrocatalytic activities.[37] However, the effect of reaction atmosphere is often ignored in the solution reaction, and there is few reports focused on the investigation of the reaction atmosphere.

Herein, the monodispersed Pd nanoparticles and its porous sphere-like aggregates were fabricated under nitrogen and air atmospheres respectively with $PdCl_2$ as the Pd precursor and hexadecylamine as reductant. The effect of the reaction atmosphere on the morphology, structure and the catalytic property of Pd was investigated.

Received: March 16, 2011
Accepted: June 23, 2011
Published: June 23, 2011

dx.doi.org/10.1021/am200330b | ACS Appl. Mater. Interfaces 2011, 3, 2425–2430

EXPERIMENTAL SECTION

Synthesis. Palladium chloride ($PdCl_2$, AR, Shanghai July Chemical Co., Ltd.) and hexadecylamine (Alfa Aesar) were used as raw materials. Before being used, hexadecylamine was dehydrated according to the following process. Zeolite and hexadecylamine were added into the flask at the mass ratio of 1:1, heated up to 80 °C, maintained at that temperature for 48 h, and then cooled to room temperature.

With the protection of a nitrogen flow, 7.727 g (32.0 mmol) hexadecylamine was melted under 100 °C to form a homogeneous liquid. Then, 0.118 g (0.67 mmol) $PdCl_2$ was added into liquid hexadecylamine and it took about 10 min to heat from 100 to 200 °C to form a light green solution. When the solution changed to opaque black after reacting for 2 min, the reaction was stopped quickly by putting the flask into cool water. The product was separated by centrifugation (9500 rpm for 5 min) and washed with hot ethanol for several times, and finally dried under vacuum at 60 °C for 2 h. The monodispersed Pd nanoparticles were obtained.

If the experiment was carried out in air atmosphere with other conditions keeping as described above, the porous sphere-like Pd aggregates would be received.

Characterization. The X-ray diffraction (XRD) patterns of the powder samples were measured at room temperature on a Rigaku D/MAX 2200PC diffractometer with CuKα (λ=0.15418 nm) radiation and graphite monochramator. The morphology and microstructure of the products were characterized using a transmission electron microscope (TEM, JEOL JEM-1230) and a high-resolution TEM (HR-TEM, JEOL JEM-2100), before observation the products were dispersed in cyclohexane. Thermal-gravimetric (TG) analysis was carried out on a Mettler Toledo SDTA851^e thermal gravimetric analyzer at a heating rate of 10.0 °C/min under air and nitrogen atmospheres. The infrared (IR) spectra were examined on a Nicolet 5DX Fourier transform infrared (FT-IR) spectrometer using the KBr pellet technique. Nitrogen adsorption−desorption data were recorded on a Quadrasorb SI apparatus at liquid nitrogen temperature (T=-196 °C). Mass spectra (MS, Agilent Q-TOF6510) were used to analyze the surface organics. The Brunauer−Emmett−Teller (BET) specific surface area was determined by a multipoint BET method using the adsorption data in the relative pressure (P/P_0) range of 0.05−0.25. Desorption isotherm was used to estimate the pore size distribution using the Barret-Joyner-Halender (BJH) theory.[38] The nitrogen adsorption volume at the relative pressure (P/P_0) of 0.970 was used to determine the pore volume and porosity.

Electrochemical Measurements. Vulcan XC 72 is one of the carbon blacks with high surface area, good electrical and thermal conductivity, suitable porosity to allow for a good reactant flow, and high stability, the large availability as well as the low cost.[39] So it was selected as the support to improve the performance of Pd catalyst. The preparation of working electrode of carbon-supported Pd catalysts is as follows. 4.0 mg of sample and 1.0 mg of Vulcan XC-72 carbon were dispersed in 300.0 μL mixed solution which contained 200.0 μL isopropanol and 100.0 μL 5 wt % Nafion solution. The mixture was sonicated for 30 min. Then 4.0 μL suspension was dropped on the glassy carbon (GC) electrode and naturally evaporated the solvent at room temperature under ambient conditions.

The electrochemical measurements were tested on CHI660 electrochemical analyzer and a conventional three-electrode electrochemical cell at room temperature. A Pt plate, the saturated calomel electrode (SCE) and the glassy carbon electrode (3.0 mm in diameter) were used as the counter electrode, the reference electrode and the working electrode, respectively. All potentials were given versus reversible hydrogen electrode (RHE) and the current densities were normalized to apparent area of the electrode.

The apparent area of Pd nanoparticles was estimated from the charge needed to form surface oxide monolayers according to the oxygen adsorption measurement method. And the value of apparent area of the working electrode was determined by dividing the amount of reduction charge by the conversion factor of 424 $\mu C/cm^2$.[40]

Voltammetric behavior of Pd nanoparticles and their electrocatalytic activity were characterized at room temperature in KOH (1.0 M) solution and KOH(1.0 M)/CH_3OH(1.0 M) mixed solution, respectively. The electrolytes were deoxygenated before each electrochemical measurement.

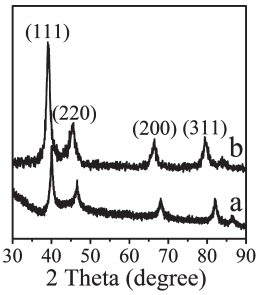

Figure 1. XRD patterns of Pd nanoparticles obtained under nitrogen (a), and air (b) atmospheres, maintaining at 200 °C for 2 min and the molar ratio of hexadecylamine to $PdCl_2$ at 48:1.

RESULTS AND DISCUSSION

The experiments were carried out under air or nitrogen atmosphere, maintaining at 200 °C for 2 min and the molar ratio of hexadecylamine to $PdCl_2$ at 48:1. The XRD pattern of the product obtained under N_2 atmosphere is shown in Figure 1a, which matches well with the face centered cubic (fcc) Pd (JCPDS, No.46−1043). In particular, the XRD pattern exhibits the typical size-broadened reflections from fcc Pd. Scherrer line width analysis of the (111) peak yields average particle size of 9.7 nm. The reflections of (111) and (220) seem a bit asymmetric, which might be due to their interaction from the further XRD analysis (Figure S1). Interestingly, the XRD reflections of the product obtained in air atmosphere shift to lower 2θ values comparing to those of fcc Pd. The characteristic diffraction peaks appearing at 39.1°, 45.6°, 66.5° and 79.5° are indexed to (111), (200), (220) and (311) lattice planes respectively. Comparing to the JCPDS data, the reflections obviously shift to lower 2θ degree, and with the angle increasing, the offset increases. That diffraction peaks downshift in 2θ (about 1° for the peak at 39.1°) indicates an increase of the lattice parameter: 0.398 nm instead of 0.389 nm in metallic Pd. Scherrer calculation gives the average crystalline size of the product obtained at air atmosphere of 8.4 nm.

Figure 2 presents the TEM and HR-TEM images of Pd nanoparticles prepared under nitrogen and air atmospheres. In the flow of nitrogen, monodispersed Pd nanoparticles with a spherical shape and an average diameter of ca.10 nm were obtained, which could be well dispersed in cyclohexane and would not aggregated for two days. The excellent dispersibility and stability of the present Pd nanoparticles might be due to the organic molecules coated on their surface. The selected area electron diffraction (SAED) pattern (the inset in Figure 2a) exhibits four clear diffraction rings, which are assigned to the (111), (200), (220), and (311) planes of fcc Pd. The HR-TEM image (Figure 2b) reveals the single crystalline nature of the monodispersed Pd nanoparticles with the (111) lattice spacing of 0.224 nm. While the experiment was carried out in the air atmosphere, three-dimensional sphere-like Pd aggregates were formed in diameter of ca.130 nm. A representative HR-TEM image (Figure 2d) shows lattice spacing

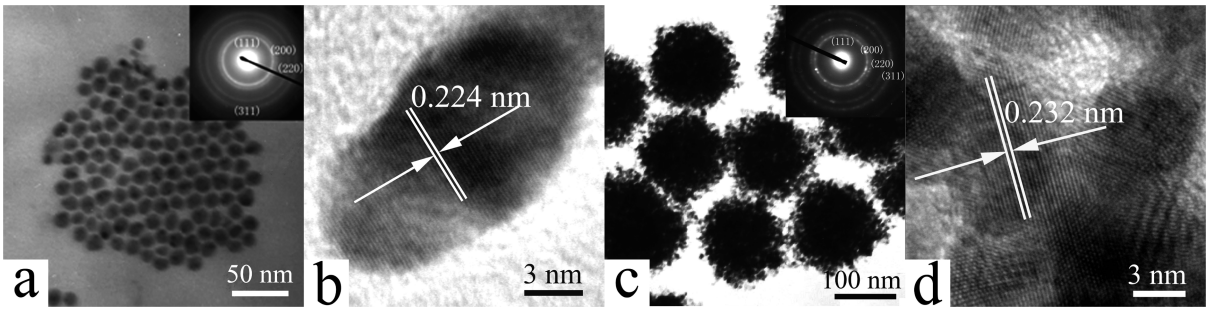

Figure 2. TEM and HR-TEM images of Pd nanoparticles obtained under (a, b) nitrogen and (c, d) air atmospheres, maintaining at 200 °C for 2 min and the molar ratio of hexadecylamine to $PdCl_2$ at 48:1. The insets in a and c are their respective SAED patterns.

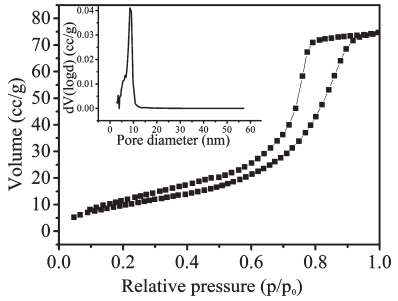

Figure 3. Nitrogen adsorption/desorption isotherms for the sample obtained in air atmosphere, and the inset is the corresponding BJH pore size distribution curve.

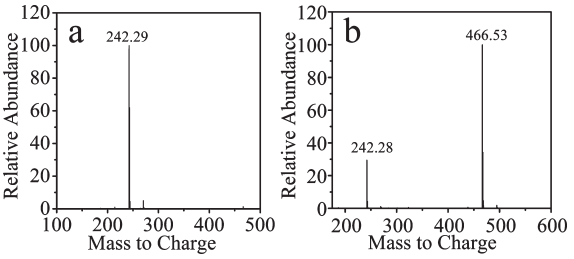

Figure 4. Mass spectra of the supernates obtained by dipping the dried samples of different atmospheres: (a) nitrogen atmosphere, (b) air atmosphere.

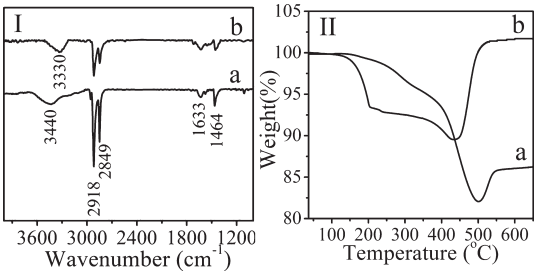

Figure 5. (I) IR spectra and (II) TG curves of the products obtained under (a) nitrogen and (b) air atmospheres.

of 0.232 nm, which is very close to the value (ca.0.229 nm) estimated by (111) lattice plane of the XRD pattern (Figure1b). The structure was aggregated randomly by small particles, and pores between these nanoparticles can be seen clearly from the images. The diameter of the primary particle was ca.6−8 nm, which was a little smaller than that calculated by Scherrer formula. This might be due to the assembly of several nanoparticles.

Figure 3 presents the nitrogen adsorption/desorption isotherms for the sample obtained in the air atmosphere, and the inset is the corresponding BJH pore size distribution curve. The adsorption isotherm belongs to a type IV curve and a type H2 hysteresis loop according to Brunauer-Deming-Deming-Teller classification,[38] indicating that the sample contains mesopores (2−50 nm). The BET specific surface area is calculated to be ca.40.1 m^2/g, and the pore volume is 0.123 cm^3/g. The corresponding BJH curve shows that the sample has a narrow pore size distribution, with the concentrated pore diameter in 8.4 nm. The pores can be attributed to the aggregation of the Pd nanoparticles, which induces the high specific surface area of the three-dimensional sphere-like aggregates.

In order to determine the surface organic precisely, the dried samples prepared under different atmospheres were dipped in cyclohexane for about half an hour. After separation, the supernates were analyzed with mass spectrometer. Major signal at 242.29 in Figure 4a is ascribed as $[C_{16}H_{33}NH_3^+]$, indicating hexadecylamine adsorbed on the surface of Pd nanoparticles obtained under N_2 atmosphere, which makes them excellent dispersibility in cyclohexane. As to air atmosphere product (Figure 4b), the signals at 242.28 and 466.53 are ascribed as $[C_{16}H_{33}NH_3^+]$ and $[(C_{16}H_{33})_2NH_2^+]$, demonstrating that the organic adsorbed on the surface of air atmosphere particles are mainly $(C_{16}H_{33})_2NH$ with a small amount of hexadecylamine. It is proposed that in the presence of oxygen and Pd catalyst the formation of $(C_{16}H_{33})_2NH$ went through the following steps, $C_{16}H_{33}NH_2 \rightarrow C_{15}H_{31}CHO \rightarrow (C_{16}H_{33})_2NH$.

IR and TG investigations are also applied to confirm the surface state of Pd nanoparticles. Figure 5I shows the IR spectra obtained by quantificationally adding the products into KBr. As to IR spectrum of the nitrogen atmosphere product (Figure 5Ia), the absorptions at 3440 cm^{-1} and 1633 cm^{-1} are respectively attributed to the stretching and rocking vibrations of N−H bonds of hexadecylamine.[41] Compared to the symmetrical (3332 cm^{-1}), asymmetrical stretching vibration (3166 cm^{-1}) and the overtone at 3255 cm^{-1} of N−H bonds of free hexadecylamine (Figure S2a), the N−H adsorptions in the IR spectrum of N_2 atmosphere product change to a broad one and shift to 3440 cm^{-1}, which reveals the covalently bonding of the N−H to the Pd surface.[42] The absorptions from 2800 cm^{-1} to 3000 cm^{-1} and that at 1464 cm^{-1} are ascribed to the vibrations of C−H bonds and weak one observed between 1250 cm^{-1} and 1020 cm^{-1} are ascribed to the C−N stretching vibrations.[41] The above analysis confirms that the monodispersed nanoparticles are covered by hexadecylamine.

After washed with cyclohexane, part of the hexadecylamine still exists from the IR spectrum (Figure S3a), which demonstrates that some of the hexadecylamine molecules are chemically bonded to the surface of Pd, and others physically adsorb on it. From the IR spectrum of the air atmosphere product (Figure 5Ib), the unsymmetrical absorptions at 3300 cm^{-1} and 1630 cm^{-1} are ascribed to the stretching and rocking vibration of N−H bonds of $(C_{16}H_{33})_2NH$ and hexadecylamine. In addition, the IR spectrum is similar to that of the oxidized hexadecylamine (Figure S2b). Therefore, the air atmosphere product is covered by $(C_{16}H_{33})_2NH$ and hexadecylamine. The absorption around 2900 cm^{-1} in curve a are much stronger than that in b, indicating that the content of organics in N_2 atmosphere product is higher than that in air atmosphere product.

The TG curve (Figure 5IIa) of monodispersed Pd nanoparticles shows that there are two obvious weight losses followed by one gain. The first drop (<300 °C, 3.36 wt %) is mainly due to the evaporation of the adsorbed hexadecylamine,[43] which can be confirmed by the IR spectrum (Figure S4) of the product calcined to 300 °C in air atmosphere with heating rate of 10 °C/min. The second one (ca.14.58 wt %) from 300 to 505 °C is overlapped with a weight gain (ca.4.06 wt %), which is ascribed to the decomposition of the chemically bonded hexadecylamine and the oxidation of Pd to PdO. When the temperature goes up to 620 °C, the product is completely oxidized to PdO, which can be confirmed by the XRD patterns of the calcined products (Figure S5). From the final weight (ca.86.12 wt %), it can be calculated that the Pd content in the initial product is ca.74.83 wt %. TG curve (curve b in Figure 5II) of the product prepared in the air atmosphere shows that the first weight loss (<300 °C, 7.50 wt %) is due to the decomposition of $(C_{16}H_{33})_2NH$ combined with the evaporation of hexadecylamine, and the second one (ca.2.95 wt %) between 300 and 440 °C is due to the decomposition of hexadecylamine. When the temperature reaches 620 °C, the sample is completely changed to its oxide. According to the final weight (ca.101.7 wt %) of the product, the content of Pd is ca.88.36 wt %. So the percentage of the organics on the surface of monodispersed Pd nanoparticle is higher than that in the air atmosphere product. More surface organic could protect the nanoparticles from being oxidized, so the starting oxidation temperature of the air atmosphere product is lower than that of nitrogen atmosphere product.

The XRD pattern of the Pd prepared in air atmosphere (Figure 1b) indicates that the lattice parameter of the Pd is larger than that of bulk metal. In order to investigate the reason why the lattice parameter of Pd prepared in air became larger, the temperatures of reaction (denoted as T_1) and molten hexadecylamine when $PdCl_2$ was added (denoted as T_2) were adjusted. As given in Figure 6, it is not difficult to find that the diffraction peaks of the products obtained at 240 °C (T_1) appear at lower angle than those obtained at 200 °C, while the temperature of molten hexadecylamine (T_2) has little effect on the position of diffraction peaks. So we can conclude that the higher the reaction temperature is, the larger the lattice parameter is, and the temperature of molten hexadecylamine when $PdCl_2$ is added has no obvious effect on it.

The observation of diffraction peaks downshift to 2θ value might origin from similar mechanism in literature. First, it could result from a uniform strain, most likely thermal, imparted to the Pd nanocrystals.[20,44,45] Alternatively, it could be a result of some other tiny atoms, such as carbon,[46] oxygen[47,48] or hydrogen[49] inserting into the lattice of Pd to form Pd solid solutions. With respect to metallic palladium, the presence of subsurface oxygen

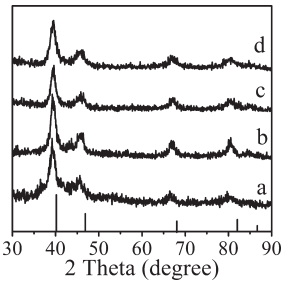

Figure 6. XRD patterns of the products obtained at different temperatures under air atmosphere. (a) T_1 = 240 °C, T_2 = 200 °C; (b) T_1 = 240 °C, T_2 = 100 °C; (c) T_1 = 200 °C, T_2 = 200 °C; (d) T_1 = 200 °C, T_2 = 100 °C.

and the incorporation of oxygen into the bulk material were investigated using DFT (density-functional theory).[50,51] The bond lengths between the subsurface O atom and its neighboring Pd atom is almost a constant value of the order of 2.0 Å. An oxygen atom in a tetrahedral interstitial site is thought to be less stable than in an octahedral site for the smaller volume in the tetrahedral site and the strong lateral expansion of the crystal lattice to achieve the optimum subsurface O−Pd bond lengths.[50] As to O atoms, occupation of interstitial sites is endothermic, so the solubility of O increases with the temperature elevating.[52,53] Together with the vast number of the available octahedral interstitial sites, a considerable amount of oxygen would deposit in the bulk material.[50] Thus, O incorporation always induces a substantial local expansion of the metallic lattice.[51]

In our experiments, the diffraction peaks of the products prepared under air atmosphere shift to lower angle obviously compared to those of fcc Pd (JCPDS, No. 46−1043), and the offset rises with the increase of reaction temperature, while the product is prepared under nitrogen atmosphere, no obvious offset can be observed from the XRD pattern. Meanwhile, the experiment is carried out under pure oxygen or compressed air atmosphere (Figure S6), the diffraction peaks of the obtained products are the same as those of the product prepared under air atmosphere. It is assumed that oxygen in air is likely to insert into the structure of metallic palladium with the growth of the nanoparticles to form the solid solution, which results in the expansion of Pd lattice.

Accordingly, we can infer the possible formation process of porous Pd nanospheres as follows. First, the Pd ions were slowly reduced by hexadecylamine to give Pd clusters in the molten solution. Then the homogeneous nucleation occurred to form the primary Pd nanoparticles when the concentration of Pd clusters reached to the critical point, and some oxygen atoms incorporated into the Pd lattice and resulted in the increasing of the lattice parameters. During the reaction, in the presence of oxygen and as-formed Pd catalyst, hexadecylamine was oxidized to its corresponding aldehyde and then the aldehyde reacted with hexadecylamine to form $(C_{16}H_{33})_2NH$. Due to its larger steric hindrance, the amount of organic molecules on the air atmosphere nanoparticles' surface is much smaller than that on the N_2 atmosphere nanoparticles' surface, which results in a relative higher surface energy of air atmosphere product and then the three-dimensional sphere-like aggregates are formed.

TG curve in N_2 atmosphere can be used to confirm O content in Pd with larger lattice parameter (denoted as PdX).[47] The nitrogen atmosphere sample was investigated by TGA measurement in the same way. When the temperature goes up to 700 °C, the weight of nitrogen atmosphere product is no longer dropping,

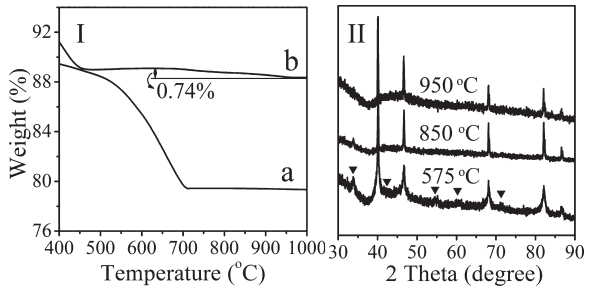

Figure 7. (I) TG curves of (a) nitrogen and (b) air atmosphere products in N_2 flow and (II) XRD patterns of sphere-like Pd aggregates calcined to different temperatures in N_2 flow.

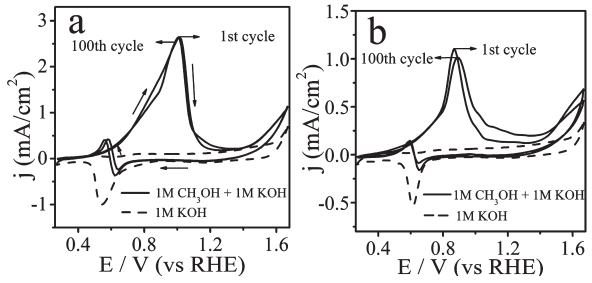

Figure 8. Cyclic voltammetry curves (CVs) for glassy carbon electrode modified with Pd nanoparticles under nitrogen in the solution of KOH (1.0 M) (dash line) and KOH (1.0 M)/CH_3OH (1.0 M) (solid line). (a) Monodispersed Pd nanoparticles, (b) sphere-like Pd aggregates. The scan rate is 50.0 mV/s, and the current is normalized to 1.0 cm^2 of apparent area.

which demonstrates that the weight loss of air atmosphere product at high temperature might be due to the removal of O in the product. In addition, the air atmosphere sample was calcined in nitrogen flow with heating rate of 10 °C/min from room temperature to 575, 850 and 950 °C. The XRD patterns of corresponding calcined products are shown in Figure 7II. When heated to 575 °C, the product is the mixture of metallic Pd and PdO, which can be due to the reaction of the dissolved oxygen atom in the lattice and the Pd atom. The slow decomposition of PdO occurred with the increase of the temperature. When calcined to 950 °C, Pd is the final product. The IR spectrum (Figure S7) indicates that the surface of the sample calcined to 620 °C is clean. Then, it is concluded that the weight loss (0.74%) from 660 to 1000 °C resulted from the decomposition of Pd oxide. Therefore, the O content in PdX can be calculated to be approximately 0.74%.

The synthesized catalysts were characterized by studies of electrochemical oxidation of methanol in alkaline electrolytes. Cyclic voltammetry technique was employed. Figure 8 shows the cyclic votammetry curves of Pd modified glassy carbon electrode in KOH (1.0 M) solution and KOH(1.0 M)/CH_3OH(1.0 M) mixed solution. The potential was scanned from 0.28 V (vs RHE) to 1.68 V (vs RHE) at the sweep rate of 50.0 mV/s. Figure 8a (solid line curve) shows the first and the 100th run voltammogram curves of the monodispersed Pd nanoparticles-modified electrode in KOH (1.0 M) solution and KOH(1.0 M)/CH_3OH(1.0 M) mixed solution. As shown in Figure 8a, the peak current of the first cycle centers at 1.01 V (vs RHE) in the forward scan, while in the reverse scan, the peak at 0.57 V (vs RHE) is observed. And no obvious oxidation peaks is observed in the absence of methanol in 1.0 M KOH (Figure 8a, dash line curve). The forward peak current density (j) is a critical parameter to measure the capacity of the catalyst. According to the experimental data, in the first cycle, the peak current for the monodispersed Pd nanoparticles is 2.64 mA/cm^2 while that for the sphere-like aggregates is only 1.09 mA/cm^2, which indicates that the monodispersed Pd nanoparticles will provide a larger working current of the fuel cell. That might be due to the higher apparent area for monodispersed Pd nanoparticles than that of sphere-like aggregates (Figure S8) and more surface defects which could be easily formed in the fast reaction.[19,27]

The carbonaceous residues formed in the electrooxidation of methanol in alkaline medium may poison the catalyst and then suppress its catalytic activity. Therefore, the stability of the methanol oxidation on the Pd electrode was investigated by cyclic voltammetry (CV) with multicycles.[54] Figure 8 shows the first and 100th cycle of the methanol electrooxidation on the catalyst of monodispersed Pd nanoparticles and its sphere-like aggregates. As to the catalyst for the monodispersed Pd nanoparticles (Figure 8a), the peak current of the first voltammegram run is 2.64 mA/cm^2 while that on the 100th run is 2.63 mA/cm^2, which reduces 0.38% compared to that of the first run. The corresponding peak currents for the sphere-like Pd aggregates are 1.09 and 1.01 mA/cm^2, which is 92.66% of the original one. Based on above analysis, it is concluded that the monodispersed Pd nanoparticles modified electrode has better catalytic activity and stability than the sphere-like aggregates.

CONCLUSIONS

We reported a facile solvothermal synthesis of Pd nanostructures by reducing $PdCl_2$ with hexadecylamine. Here, different atmospheres resulted in Pd with different morphologies and lattice parameters. Furthermore, we explained the aggregation of Pd nanoparticles and the expansion of lattice parameters, finding that oxygen played an important role in the formation of the porous sphere-like Pd and the expansion of its lattice parameters respectively by changing surface groups and incorporating into the Pd metal. The electrocatalytic activity between monodispersed Pd nanoparticles and its porous sphere-like aggregates for the oxidation of methanol was compared, showing that the monodispersed Pd nanoparticles exhibited superior catalytic performance and good stability.

ASSOCIATED CONTENT

Supporting Information. Monodispersed Pd nanoparticles' XRD patterns obtained by slowly scanning from 35 to 55°, IR spectra of pure hexadecylamine and the oxidation product of hexadecylamine, IR spectra of the sample prepared under different atmosphere after being washed with cyclohexane, IR spectra and XRD patterns of the samples calcined from room temperature to different temperature; TEM image and XRD patterns of Pd nanoparticles obtained under oxygen atmosphere and cyclic voltammetry curves (CVs) for glassy carbon electrode modified with Pd under nitrogen in the solution of 1.0 M H_2SO_4 (PDF). This material is available free of charge via the Internet at http://pubs.acs.org.

AUTHOR INFORMATION

Corresponding Author

*E-mail: jiaoxl@sdu.edu.cn. Fax:+86-0531-88364281. Tel: +86-0531-88364280.

■ ACKNOWLEDGMENT

This work is supported by the 973 program of the Ministry of Science and Technology of China (2010CB933504) and the Science Funds for Distinguished Young Scientists of Shandong Province (JQ200903).

■ REFERENCES

(1) Teschner, D.; Borsodi, J.; Wootsch, A.; Révay, Z.; Hävecker, M.; Knop-Gericke, A.; Jackson, S. D.; Schlögl, R. *Science* **2008**, *320*, 86.
(2) Narayanan, R.; El-Sayed, M. A. *Langmuir* **2005**, *21*, 2027.
(3) Schlapbach, L.; Züttel, A. *Nature* **2001**, *414*, 353.
(4) Yamauchi, M.; Ikeda, R.; Kitagawa, H.; Takata, M. *J. Phy. Chem. C* **2008**, *112*, 3294.
(5) Yang, F.; Taggart, D. K.; Penner, R. M. *Nano Lett.* **2009**, *9*, 2177.
(6) Favier, F.; Walter, E. C.; Zach, M. P.; Benter, T.; Penner, R. M. *Science* **2001**, *293*, 2227.
(7) Sun, Y.; Wang, H. H. *Adv. Mater.* **2007**, *19*, 2818.
(8) Cherevko, S.; Kulyk, N.; Fu, J.; Chung, C.-H. *Sensor Actuat. B: Chem* **2009**, *136*, 388.
(9) Xia, Y.; Xiong, Y.; Lim, B.; Skrabalak, S. E. *Angew. Chem., Int. Ed.* **2009**, *48*, 60.
(10) Tao, A. R.; Habas, S.; Yang, P. *Small* **2008**, *4*, 310.
(11) Nishihata, Y.; Mizuki, J.; Akao, T.; Tanaka, H.; Uenishi, M.; Kimura, M.; Okamoto, T.; Hamada, N. *Nature* **2002**, *418*, 164.
(12) Tian, N.; Zhou, Z.-Y.; Sun, S.-G.; Ding, Y.; Wang, Z. L. *Science* **2007**, *316*, 732.
(13) Sau, T. K.; Rogach, A. L. *Adv. Mater.* **2010**, *22*, 1781.
(14) Sau, T. K.; Rogach, A. L.; Jäckel, F.; Klar, T. A.; Feldmann, J. *Adv. Mater.* **2010**, *22*, 1805.
(15) Piao, Y.; Jang, Y.; Shokouhimehr, M.; Lee, I. S.; Hyeon, T. *Small* **2007**, *3*, 255.
(16) Wilson, O. M.; Knecht, M. R.; Garcia-Martinez, J. C.; Crooks, R. M. *J. Am. Chem. Soc.* **2006**, *128*, 4510.
(17) Ratke, L.; Voorhees, P. W. *Dordrecht* **2002**, 117.
(18) Durand, J.; Teuma, E.; Gómez, M. *Eur. J. Inorg. Chem.* **2008**, 3577.
(19) Mazumder, V.; Sun, S. *J. Am. Chem. Soc.* **2009**, *131*, 4588.
(20) Teranishi, T.; Miyake, M. *Chem. Mater.* **1998**, *10*, 594.
(21) Chiu, C.-Y.; Li, Y.; Huang, Y. *Nanoscale* **2010**, *2*, 927.
(22) Huang, X.; Zheng, N. *J. Am. Chem. Soc.* **2009**, *131*, 4602.
(23) Xiong, Y.; Cai, H.; Wiley, B. J.; Wang, J.; Kim, M. J.; Xia, Y. *J. Am. Chem. Soc.* **2007**, *129*, 3665.
(24) Xiao, C.; Ding, H.; Shen, C.; Yang, T.; Hui, C.; Gao, H.-J. *J. Phy. Chem. C* **2009**, *113*, 13466.
(25) Liang, H.-W.; Liu, S.; Gong, J.-Y.; Wang, S.-B.; Wang, L.; Yu, S.-H. *Adv. Mater.* **2009**, *21*, 1850.
(26) Xiong, Y.; McLellan, J. M.; Chen, J.; Yin, Y.; Li, Z.-Y.; Xia, Y. *J. Am. Chem. Soc.* **2005**, *127*, 17118.
(27) Yin, Z.; Zheng, H.; Ma, D.; Bao, X. *J. Phy. Chem. C* **2009**, *113*, 1001.
(28) Zhou, P.; Dai, Z.; Fang, M.; Huang, X.; Bao, J.; Gong, J. *J. Phy. Chem. C* **2007**, *111*, 12609.
(29) Fan, F.-R.; Attia, A.; Sur, U. K.; Chen, J.-B.; Xie, Z.-X.; Li, J.-F.; Ren, B.; Tian, Z.-Q. *Cryst. Growth Des.* **2009**, *9*, 2335.
(30) Zhou, G.; Lu, M.; Yang, Z.; Tian, F.; Zhou, Y.; Zhang, A. *Cryst. Growth Des.* **2007**, *7*, 187.
(31) Gugliotti, L. A.; Feldheim, D. L.; Eaton, B. E. *Science* **2004**, *304*, 850.
(32) Gugliotti, L. A.; Feldheim, D. L.; Eaton, B. E. *J. Am. Chem. Soc.* **2005**, *127*, 17814.
(33) Lim, B.; Xiong, Y.; Xia, Y. *Angew. Chem., Int. Ed.* **2007**, *46*, 9279.
(34) Lim, B.; Jiang, M.; Tao, J.; Camargo, P. H. C.; Zhu, Y.; Xia, Y. *Adv. Func. Mater.* **2009**, *19*, 189.
(35) Choo, H.; He, B.; Liew, K. Y.; Liu, H.; Li, J. *J. Mol. Catal A: Chem.* **2006**, *244*, 217.
(36) Watt, J.; Young, N.; Haigh, S.; Kirkland, A.; Tilley, R. D. *Adv. Mater.* **2009**, *21*, 2288.
(37) Li, H.; Sun, G.; Gao, Y.; Jiang, Q.; Jia, Z.; Xin, Q. *J. Phy. Chem. C* **2007**, *111*, 15192.
(38) Sing, K. S. W.; Everett, D. H.; Haul, R. A. W.; Pierotti, R. A.; Rouquérol, J.; Siemieniewska, T. *Pure Appl. Chem.* **1985**, *57*, 603.
(39) Bianchini, C.; Shen, P. K. *Chem. Rev.* **2009**, *109*, 4183.
(40) Pan, W.; Zhang, X.; Ma, H.; Zhang, J. *J. Phy. Chem. C* **2008**, *112*, 2456.
(41) Wang, H.; Jiao, X.; Chen, D. *J. Phy. Chem. C* **2008**, *112*, 18793.
(42) Meulenberg, R. W.; Strouse, G. F. *J. Phys. Chem. B* **2001**, *105*, 7438.
(43) Yao, K. X.; Yin, X. M.; Wang, T. H.; Zeng, H. C. *J. Am. Chem. Soc.* **2010**, *132*, 6131.
(44) Heinemann, K.; Poppa, H. *Surf. Sci.* **1985**, *156*, 265.
(45) Lineberry, Q. J.; Cao, Y.; Lin, Y.; Ghose, S.; Connell, J. W.; Pan, W.-P. *Energ Fuel* **2009**, *23*, 1512.
(46) Lamber, R.; Jaeger, N.; Schulz-Ekloff, G. *Surf. Sci.* **1990**, *227*, 15.
(47) Maillet, T.; Solleau, C.; Barbier, J., Jr; Duprez, D. *Appl. Catal. B: Environ.* **1997**, *14*, 85.
(48) Ferhat-Hamida, Z.; Barbier, J.; Labruquere, S.; Duprez, D. *Appl. Catal. B: Environ.* **2001**, *29*, 195.
(49) Kuhrt, C.; Anton, R. *Thin Solid Films* **1991**, *198*, 301.
(50) Todorova, M.; Reuter, K.; Scheffler, M. *Phys. Rev. B* **2005**, *71*, 195403.
(51) Todorova, M.; Li, W. X.; Ganduglia-Pirovano, M. V.; Stampfl, C.; Reuter, K.; Scheffler, M. *Phy. Rev. Lett.* **2002**, *89*, 096103.
(52) Wang, D.; Flanagan, T. B. *Scripta Mater.* **2005**, *52*, 599.
(53) Gegner, J.; Hörz, G.; Kirchheim, R. *J. Mater. Sci.* **2009**, *44*, 2198.
(54) Su, L.; Jia, W.; Schempf, A.; Ding, Y.; Lei, Y. *J. Phy. Chem. C* **2009**, *113*, 16174.